Combustion and Flame

Pyrolysis effects during high-temperature vaporization of alkane droplets

--Manuscript Draft--

Manuscript Number:	CNF-D-19-00972R3
Article Type:	Full Length Article
Keywords:	Droplet vaporization; fuel pyrolysis; activation-energy asymptotics
Corresponding Author:	Álvaro Muelas CSIC – University of Zaragoza Zaragoza, SPAIN
First Author:	Álvaro Muelas
Order of Authors:	Álvaro Muelas
	Jaime Carpio, Professor
	Javier Ballester, Professor
	Antonio Luis Sánchez, Professor
	Forman Arthur Williams, Professor
Abstract:	The temporal evolution of the droplet radius is measured experimentally in high-temperature inert atmospheres for three different alcohols (ethanol, n-butanol, and glycerol) and three alkanes (n-heptane, n-dodecane, and n-hexadecane). It is shown that, while accompanying theoretical predictions of droplet-radius variations show excellent accuracy for the three alcohols, the three alkanes exhibit vaporization rates that are significantly smaller than those predicted theoretically. The accompanying observation of significant soot formation suggests that endothermic fuel pyrolysis may be responsible for the diminished vaporization rate. The quantification of this phenomenon is investigated here using a one-step irreversible reaction with an Arrhenius rate to model the fuel decomposition. It is shown how an analytical description developed on the basis of activation-energy asymptotics can be used in combination with the experimental measurements of the temporal droplet-radius evolution to adjust the fuel-pyrolysis kinetics, embodied at leading order in an effective pyrolysis temperature, which is obtained for n-heptane, n-dodecane, and n-hexadecane.

Pyrolysis effects during high-temperature vaporization of alkane droplets.

Álvaro Muelas[a], Jaime Carpio[b], Javier Ballester[c], Antonio L. Sánchez[d], Forman A. Williams[d]

[a]*Laboratory of Research on Fluid Dynamics and Combustion Technologies (LIFTEC), CSIC–University of Zaragoza, Spain*
[b]*E. T. S. I. Industriales, Universidad Politécnica de Madrid, Madrid, 28006, Spain*
[c]*Fluid Mechanics Group/LIFTEC, School of Engineering and Architecture, CSIC-University of Zaragoza, María de Luna, 3, 50018 Zaragoza, Spain*
[d]*Dept. Mechanical and Aerospace Engineering, University of California San Diego, La Jolla CA 92093-0411, USA*

Abstract

The temporal evolution of the droplet radius is measured experimentally in high-temperature inert atmospheres for three different alcohols (ethanol, n-butanol, and glycerol) and three alkanes (n-heptane, n-dodecane, and n-hexadecane). It is shown that, while accompanying theoretical predictions of droplet-radius variations show excellent accuracy for the three alcohols, the three alkanes exhibit vaporization rates that are significantly smaller than those predicted theoretically. The accompanying observation of significant soot formation suggests that endothermic fuel pyrolysis may be responsible for the diminished vaporization rate. The quantification of this phenomenon is investigated here using a one-step irreversible reaction with an Arrhenius rate to model the fuel decomposition. It is shown how an analytical description developed on the basis of activation-energy asymptotics can be used in combination with the experimental measurements of the temporal droplet-radius evolution to adjust the fuel-pyrolysis kinetics, embodied at leading order in an effective pyrolysis temperature, which is obtained for n-heptane, n-dodecane, and n-hexadecane.

Keywords: Droplet vaporization, fuel pyrolysis, activation-energy asymptotics

1. Introduction

Because of its numerous related applications, the problem of individual-droplet vaporization has been studied at length (see, e.g., [1, 2] for reviews). Although the initial work focused on isothermal evaporation of a drop surrounded by an atmosphere at the same temperature, attention soon turned to the problem of a droplet vaporizing in a hot atmosphere [3, 4], that being especially of interest in combustion applications. Useful analytical expressions for the rate of droplet vaporization were reported by Godsave and Spalding at the fourth combustion symposium [5, 6]. These early modeling efforts have been complemented

over the years to account for effects of relative droplet-gas motion, multicomponent composition of liquid fuels, and internal circulation of the liquid, as described, for example, in [7].

In most spray-combustion applications, droplets primarily burn in a group-combustion regime, with the fuel that originates from the vaporizing droplets burning with the ambient oxygen in a flame that surrounds the droplet cloud (see [8] for a recent review of spray combustion). Since fuel oxidation in the atmosphere surrounding each individual droplet (i.e. at distances of the order of the droplet radius) is negligibly small in the group-combustion regime, theories addressing droplet vaporization in a hot inert atmosphere [9] provide adequate quantification of the resulting droplet vaporization rate for spray-combustion computations. The present paper explores vaporization-rate departures encountered in liquid-hydrocarbon droplets when the ambient thermal conditions promote significant pyrolysis of the fuel vapor. As explained below, this effect becomes significant at high ambient temperatures exceeding about 1000 K, often encountered in liquid-fuel burners, when the characteristic time of thermal hydrocarbon decomposition becomes comparable to the characteristic diffusion time around the droplet. Under those conditions, a significant fraction of the heat transferred from the hot atmosphere is employed to pyrolyze the fuel, thereby reducing the amount of heat available to heat up and vaporize the liquid fuel.

The motivation for the present study is to help to ascertain how accurately classical theories of droplet vaporization can be applied in describing the spray combustion processes that occur in the group-combustion regime. Since transient droplet evaporation is likely to be of relevance in the interior of groups under such conditions, experiments were designed under which time-dependent effects are significant. Comparisons of measured and computed histories can test how well the theoretical descriptions perform. For some fuels, soot formation through fuel pyrolysis may occur during group combustion in the outer portions of the group, where the temperatures of the gases surrounding the droplets are higher. Excessive soot formation generally is detrimental, and the extent to which it may be present and interact with the droplet vaporization processes is poorly understood. Soot-production chemistry may occur either in the inner quasi-steady zone that develops around a droplet during the later stages of evaporation or in outer fully transient zones [10] farther away from the droplets in the spray. The present investigation addresses, for the first time, the first of these two possibilities, offering a new theoretical simplification that may prove useful in future analyses of spray combustion in the group-combustion regime. The new theoretical description, motivated by the present experimental measurements, may impact future computational investigations of spray combustion, leading to improved fidelity in combustor designs.

The paper begins by presenting illustrative experimental results corresponding to alcohol and alkane droplets vaporizing in a hot inert atmosphere. The measured temporal variation of the droplet radius is compared with standard predictions based on a chemistry-free droplet-vaporization model, yielding excellent agreement for alcohol vaporization. For the alkane droplets, however, the predictions show significant departures from the experimental measurements, with relative differences being more pronounced for heavier fuel molecules and also at higher ambient temperatures. The reduced vaporization rate measured in the

experiments is attributed here to decreased rates of heat transfer to the liquid caused by endothermic fuel pyrolysis, consistent with the appearance of soot, which was observed in all alkane experiments. In an effort to improve quantification of the process, a new theory of droplet vaporization in the presence of fuel pyrolysis is developed here. The strong temperature sensitivity of the pyrolytic reactions is exploited in our large-activation-energy analysis, with the fuel decomposition occurring in a thin layer at a fixed pyrolysis temperature, a property of the fuel whose approximate value is evaluated from the vaporization rate measured experimentally.

2. Experimental measurements

Six different fuels were employed in this study, namely three alcohols (ethanol, n-butanol, and glycerol) and three alkanes (n-heptane, n-dodecane, and n-hexadecane). All the samples used in the tests were above 99.0 % in purity. The evaporation process of these liquid-fuel droplets was studied in the Droplet Combustion Facility (DCF) available at LIFTEC, represented schematically in Fig. 1. Since a detailed description of this facility can be found in a recent publication [11], only its most relevant features will be given below.

A stream of free-falling droplets was generated at a piezoelectric device, with droplet initial radii (a_0) of 72.5 μm for ethanol and butanol and 75 μm for the rest of fuels. It is noteworthy that these radii are in a range often encountered in practical applications, while larger droplets often had to be employed in other experimental investigations. The droplet-generation frequency was fixed at 25 Hz, providing interdroplet distances large enough to avoid interactions between droplets [12]. The droplet-generation steadiness was thoroughly checked, primarily at the first position that allowed optical access to the combustion chamber (i.e., 3 mm below the droplet injection point), yielding a deviation in a_0 as low as 0.3 μm throughout the course of the experiments (rms value for all the tests). Glycerol had to be preheated to 100^o C prior to its atomization in order to lower its viscosity, whereas the rest of the fuels were atomized at room temperature.

The droplets were injected into the inert combustion products of a McKenna flat-flame burner, which provided the inert hot coflow required for the liquid-fuel evaporation and pyrolysis. This burner was fed with different stoichiometric mixtures of CH_4, H_2, O_2, CO_2, and air, as to provide a coflow gas mixture of N_2, CO_2, and H_2O at the desired temperature T_∞. Since the droplets are injected through an orifice, this target temperature T_∞ is achieved at a finite distance of the order of 10 mm from the burner. Further downstream the temperature along the droplet trajectory remains equal to T_∞, as verified in temperature measurements with a thin S-type thermocouple having a 50-μm diameter (see Appendix C of the Supplementary materials of [11] for details of the temperature profile).

All fuels were tested for a target temperature $T_\infty = 1730$ K. Additionally, hexadecane was also tested at a lower target temperature, $T_\infty = 1311$ K, achieved by modifying the reactant feed to the flat-flame burner. In these inert gas mixtures, the vaporization of alcohol droplets proceeds with negligible chemical activity. For alkane droplets, however, significant fuel pyrolysis is present at the high temperatures employed in the experiments, as revealed by the appearance of visible soot traces, shown in Fig. 1b for heptane and

dodecane. As discussed below, the endothermic fuel decomposition has an important effect on the resulting vaporization rate.

The coflow velocity was measured for the standard coflow condition $T_\infty = 1730$ K by means of the PIV technique using a Nd:YAG laser with Al_2O_3 0.3 μm particles as tracers, thereby allowing quantification of the relative droplet-coflow velocity. The optical setup was fixed, the flat-flame burner being moved vertically to vary the residence time of the droplet in the hot gas prior to measurement. The droplet vaporization process was measured by images acquired with a backlit CCD camera (QImaging Retiga SRV) fitted with a long-distance microscope, which was employed to determine both the size and velocity histories of the free-falling droplets. The spatial resolution for this optical setup was 1.4 μm/pixel, allowing us to capture with good accuracy droplets above 25 μm in diameter. The backlight used was an LED stroboscope programmed to shoot sequential flashes every 0.5 ms. This, in combination with the exposure time of the camera, permitted recording of two sequential shots of the same droplet in each photograph, as displayed in Fig. 1c. Subsequent automatic post-processing of these images was carried out in Matlab to extract the droplet sizes and velocities in a precise and repeatable way. Associated Reynolds numbers for the flow around the droplet were found to be smaller than 0.5 throughout the entire recorded droplet lifetimes, with typical values on the order of 0.2 during most of the droplet vaporization history. The results of the droplet measurements provide the variation of the squared droplet radius a^2 with the residence time t in the hot gas, represented by symbols in Fig. 2 for the six fuels considered here (the accompanying curves in the figure correspond to theoretical predictions, to be discussed below).

As can be inferred from the curves in Fig. 2, vaporization is negligible during the initial droplet heat-up period, which is longer for fuels with higher boiling temperature (i.e. glycerol, dodecane, and hexadecane). For these fuels, the decrease in the liquid-fuel density associated with the temperature increase leads to a noticeable increase in the droplet radius during this stage. Vaporization begins once the droplet-surface temperature reaches a value close to the boiling temperature and continues until the droplet disappears. As expected, most of the vaporization occurs with a constant slope $\mathrm{d}a^2/\mathrm{d}t$, achieved when the droplet reaches a uniform constant temperature.

3. Predictions of droplet vaporization

The experimental measurements of the droplet-radius temporal evolution $a(t)$ were compared with theoretical predictions obtained following the standard theory of droplet vaporization in an inert environment at temperature T_∞ [7]. For the small values of the droplet Reynolds number found in the experiments, corrections associated with forced-convection effects remain negligibly small, so that the flow is effectively spherico-symmetrical. Correspondingly, all variables are functions of the time t and the radial distance $\tilde{r}$ to the droplet center. The evolution of the temperature inside the droplet $T_l(\tilde{r}, t)$ from its initial uniform value $T_l(\tilde{r}, 0) = T_0$ was computed by integration of the energy equation

$$\rho_l c_l \frac{\partial T_l}{\partial t} = \frac{1}{\tilde{r}^2}\frac{\partial}{\partial \tilde{r}}\left(\kappa_l \tilde{r}^2 \frac{\partial T_l}{\partial \tilde{r}}\right) \left\{ \begin{array}{ll} \tilde{r} = 0: & \frac{\partial T_l}{\partial \tilde{r}} = 0 \\ \tilde{r} = a: & 4\pi\kappa_l a^2 \frac{\partial T_l}{\partial \tilde{r}} = \dot{q}_d \end{array} \right. \quad (1)$$

while the droplet radius $a(t)$ is computed from the integrated form of the continuity equation

$$\frac{\mathrm{d}}{\mathrm{d}t}\left(4\pi\int_0^a \rho_l \tilde{r}^2 \mathrm{d}\tilde{r}\right) = -\dot{m}, \tag{2}$$

subject to the initial condition $a(0) = a_0$. The density ρ_l, specific heat c_l, and thermal conductivity κ_l of the liquid fuel are functions of the temperature.

The droplet vaporization rate $\dot{m}$ and the droplet heating rate $\dot{q}_d$ appearing above are determined from the analysis of the quasi-steady spherico-symmetrical structure of the gas flow surrounding the droplet, which can be described in terms of the gas temperature T and fuel-vapor mass fraction Y. For the cases considered here, corrections arising from unsteady gas-phase effects, scaling with the inverse square root of the liquid-to-ambient density ratio [10], remain small, and have been correspondingly neglected in our analysis. The solution depends on the value of the droplet-surface temperature T_s, related to the surface value of the fuel-vapor mass fraction Y_s by the Clasius-Clapeyron relation

$$Y_s = \left[Y_s + \frac{M_F}{M_I}(1 - Y_s)\right] \exp\left[\frac{L_v}{R_F T_B} - \frac{L_v}{R_F T_s}\right] \tag{3}$$

involving the molecular masses of the fuel and the inert M_F and M_I, the boiling temperature T_B, the latent heat of vaporization L_v, and the fuel constant $R_F = R_o/M_F$, with R_o representing the universal gas constant. To facilitate the description, the analysis is carried out by assuming that the gas thermal conductivity κ, specific heat at constant pressure c_p, and fuel Lewis number $L = \kappa/(\rho c_p D)$, with D denoting the fuel-vapor diffusivity, take uniform values, obtained with use of the so-called "1/3 rule" [13], as explained below. The accuracy of this widely used approximation in describing alcohol and alkane droplet vaporization was tested by comparisons with numerical integrations accounting for the variation of κ, c_p, and L with temperature and composition. For the conditions considered below, the observed differences in resulting vaporization rates were found to be negligibly small, in agreement with early findings [13], thereby justifying the adoption of this constant-property simplification.

Integration of the energy and fuel-vapor conservation equations, subject to the boundary conditions $T = T_s$ and $Y = Y_s$ at $\tilde{r} = a$ and $T = T_\infty$ and $Y = 0$ as $\tilde{r} \to \infty$, leads to the familiar expressions

$$\lambda = \frac{\dot{m}}{4\pi\kappa a/c_p} = \frac{1}{L}\ln\left(\frac{1}{1 - Y_s}\right) \tag{4}$$

for the dimensionless vaporization rate λ and

$$\frac{\dot{q}_d}{4\pi\kappa a L_v/c_p} = \lambda\left[\frac{c_p(T_\infty - T_s)/L_v}{e^\lambda - 1} - 1\right] \tag{5}$$

for the dimensionless droplet heating rate.

The above expressions (4) and (5), supplemented with (3), are used in integrating (1) and (2). Following standard practice [13], properties of the fuel-inert gas mixture are evaluated using reference values of the temperature $T_{\mathrm{ref}} = T_s + (T_\infty - T_s)/3$ and fuel mass fraction

$Y_{\rm ref} = 2Y_s/3$. For example, the density ρ is computed at $T_{\rm ref}$ as that of an ideal gas mixture of fuel and inert with mass fractions $Y_{\rm ref}$ and $1-Y_{\rm ref}$, respectively. The thermal conductivity κ and the fuel diffusivity D are evaluated using mixture-average expressions [14], with the thermal conductivity of each gaseous species and the binary diffusivity of the fuel into each inert species evaluated at the reference temperature $T_{\rm ref}$. The specific heat c_p is taken to be that of the fuel vapor at $T_{\rm ref}$ [13].

The evolution of the droplet radius with time, obtained from integrations of the above problem for the six fuels considered here, is shown in the curves of Fig. 2, where the small effects of initial departures from the target temperature T_∞ have been taken into account. As can be anticipated from (3), since $L_v \gg R_F T_B$ for all fuels tested here, with the injection droplet temperature T_0 being significantly below the boiling temperature T_B (i.e. for $(T_B - T_0)/T_B \gg [L_v/(R_F T_B)]^{-1}$), the fuel-vapor mass fraction at the droplet surface is initially negligible. During this initial stage it is thus found from (4) that $\lambda \simeq 0$, while the droplet heating rate is $\dot{q}_d = 4\pi\kappa a(T_\infty - T_s)$, as follows from (5). During this heat-up period the droplet mass, $4\pi \int_0^a \rho_l \tilde{r}^2 {\rm d}\tilde{r}$, remains constant, but its radius increases as a result of the decreasing liquid-fuel density $\rho_l(T_l)$. Significant vaporization begins to occur as T_s reaches values such that $(T_B - T_s)/T_B \sim [L_v/(R_F T_B)]^{-1}$. As vaporization proceeds further, a stage is reached in which the temperature inside the droplet reaches a constant uniform value equal to T_s and the reduced vaporization rate reaches the familiar Spalding value [5, 6]

$$\lambda = \ln\left(1 + \frac{c_p(T_\infty - T_s)}{L_v}\right), \tag{6}$$

as follows from (5) when $\dot{q}_d = 0$, with corresponding constant values of T_s and Y_s, determined from (3) and (4). During this final vaporization stage the mass-conservation equation (2) reduces to the so-called d^2-law

$$\frac{{\rm d}a^2}{{\rm d}t} = -\frac{2\kappa}{\rho_l c_p}\lambda, \tag{7}$$

so that the curves representing the variation with time of the square of the droplet radius become straight lines with negative slope.

As can be observed in Fig. 2, the agreement between the droplet vaporization model and the experiments is remarkably good for the three alcohols, whereas for alkanes the model tends to over-predict the vaporization rate, with over-predictions becoming larger for larger molecular weight. The departures are especially noticeable during the final stage, with the model consistently over-predicting the constant slope $-{\rm d}a^2/{\rm d}t$. In order to quantify these deviations, the curves shown in Fig. 2 were fitted to straight lines using the least-squared method to extract the quasi-steady vaporization rates of the different fuels. The selected interval for this fitting was $0.2 \leq (a/a_0)^2 \leq 0.6$, a convenient intermediate region, where the initial heating transient can be considered to be essentially completed while the droplet radius is large enough to avoid the higher experimental uncertainties related to the measurement of very small droplets. The values of $-{\rm d}a^2/{\rm d}t$ extracted from the experiments are listed in Table 1 along with the theoretical predictions. It can be seen in the table that the theoretical predictions and the experimentally measured values are in excellent agreement

for the three alcohols, with relative errors remaining below 5% in all three cases. By way of contrast, the experimentally measured values for the three alkanes differ significantly from the corresponding theoretical predictions. The largest departures correspond to hexadecane at high temperature.

The reduced vaporization rate seems to indicate that the alkane droplets effectively see an ambient temperature that is lower than the actual ambient temperature of the coflow. This, along with the observation of soot formation, is consistent with the presence of endothermic pyrolysis. The needed theoretical description of the problem is given below.

Values of $-\mathrm{d}a^2/\mathrm{d}t$ (mm^2/s)		
Fuel	Experiments	Theoretical predictions
Ethanol	0.1001	0.1049
Butanol	0.1093	0.1137
Glycerol	0.0781	0.0756
Heptane	0.1363	0.1537
Dodecane	0.1337	0.1639
Hexadecane ($T_\infty = 1730$ K)	0.1329	0.1771
Hexadecane ($T_\infty = 1311$ K)	0.1156	0.1352

4. A model for droplet vaporization with fuel-vapor pyrolysis

If the ambient temperature is high enough, the gaseous alkane molecules C_nH_{2n+2} may decompose into smaller molecules through an endothermic process that lowers the gas temperature. The associated thermal kinetics is known to involve numerous elementary reactions [15]. The dominant pathway and the resulting products arising from decomposition of a given fuel depend on the combustion conditions. All of these complicating details do not need to be accounted for in our analysis, focused on global effects arising from the endothermic nature of the thermal hydrocarbon pyrolysis chemistry. Instead, for our purposes it suffices to model the pyrolytic kinetics with a single irreversible reaction, with the associated energetics evaluated by assuming that C_2H_4 is the main product of pyrolysis. Depending on the number of carbon atoms n present in the alkane molecule, the overall reaction is either $C_nH_{2n+2} \rightarrow \frac{n-1}{2}C_2H_4 + CH_4$ (when n is odd) or $C_nH_{2n+2} \rightarrow \frac{n-2}{2}C_2H_4 + C_2H_6$ (when n is even). The amount of heat needed to pyrolyze a unit mass of fuel vapor q can be correspondingly obtained from the enthalpies of formation of C_nH_{2n+2}, C_2H_4, CH_4, and C_2H_6 to give, for instance, $q = (2.70, 2.75, 2.90)$ MJ/kg for heptane, dodecane, and hexadecane, respectively. These values are much smaller than the associated heat of combustion, slightly above 47 MJ/kg for all three fuels, but much larger than their latent heat of vaporization at T_B, given by $L_v = (0.313, 0.261, 0.224)$ MJ/kg for heptane, dodecane, and hexadecane.

The fuel decomposition rate ω (mass of fuel consumed per unit volume per unit time) will be modeled with the Arrhenius expression

$$\omega = \rho B Y \exp\left(-\frac{E_a}{R_o T}\right), \tag{8}$$

where ρ is the density and B and E_a are the preexponential frequency factor and activation energy, respectively. For constant values κ, c_p, and $L = \kappa/(\rho c_p D)$ the problem reduces to that of integrating

$$\frac{\lambda}{r^2}\frac{\mathrm{d}Y}{\mathrm{d}r} - \frac{1}{L}\frac{1}{r^2}\frac{\mathrm{d}}{\mathrm{d}r}\left(r^2\frac{\mathrm{d}Y}{\mathrm{d}r}\right) = -\frac{B}{\kappa/(\rho c_p a^2)}Y\exp\left(-\frac{E_a}{R_o T}\right), \tag{9}$$

$$\frac{\lambda}{r^2}\frac{\mathrm{d}}{\mathrm{d}r}(c_pT/q) - \frac{1}{r^2}\frac{\mathrm{d}}{\mathrm{d}r}\left(r^2\frac{\mathrm{d}}{\mathrm{d}r}(c_pT/q)\right) = -\frac{B}{\kappa/(\rho c_p a^2)}Y\exp\left(-\frac{E_a}{R_o T}\right), \tag{10}$$

with boundary conditions

$$T(1) - T_s = Y(1) - Y_s = 0 \quad \text{and} \quad T(\infty) - T_\infty = Y(\infty) = 0. \tag{11}$$

Here $r = \tilde{r}/a$ represents the radial distance to the center of the droplet scaled with the droplet radius. The rescaled vaporization rate λ defined in the first equation of (4) appears as an eigenvalue, to be determined with the additional mass-conservation condition

$$\lambda = \lambda Y_s - \frac{1}{L}\left.\frac{\mathrm{d}Y}{\mathrm{d}r}\right|_{r=1} \tag{12}$$

at the droplet surface, where energy conservation provides

$$\frac{\dot{q}_d}{4\pi\kappa a L_v/c_p} + \lambda = \frac{c_p}{L_v}\left.\frac{\mathrm{d}T}{\mathrm{d}r}\right|_{r=1}, \tag{13}$$

which serves to determine $\dot{q}_d$, thereby completing the solution. In solving (9)–(11) it is sometimes convenient to replace either (9) or (10) by the chemistry-free combination

$$\frac{\mathrm{d}}{\mathrm{d}r}\left\{\lambda\left[\frac{c_pT}{q} - Y\right] - \frac{\mathrm{d}}{\mathrm{d}r}\left[r^2\left(\frac{c_pT}{q} - \frac{Y}{L}\right)\right]\right\} = 0, \tag{14}$$

to be used later in the course of the solution. As expected, the above formulation reproduces the classical droplet-vaporization results in the absence of chemical reaction, when (9) and (10) can be readily integrated to give the expressions

$$\frac{Y}{Y_s} = \frac{1 - e^{-L\lambda/r}}{1 - e^{-L\lambda}} \quad \text{and} \quad \frac{T - T_\infty}{T_s - T_\infty} = \frac{1 - e^{-\lambda/r}}{1 - e^{-\lambda}}, \tag{15}$$

which can be used in (12) to yield (4) for the dimensionless vaporization rate and in (13) to yield (5) for the droplet heating rate.

5. Solution for large activation energies

5.1. Preliminary considerations

As seen in the dimensionless equations (9) and (10), the relative importance of the chemical reaction is measured by the ratio of the characteristic diffusion time in the gas surrounding the droplet $La^2/[\kappa/(\rho c_p)] = a^2/D$ to the characteristic value of the fuel-consumption

time $\{B\exp[-E_a/(R_oT)]\}^{-1}$. For large values of the activation energy E_a the chemical reaction displays a strong dependence on the temperature, so that for configurations with $T_\infty - T_s \sim T_\infty$, the case considered here, the fuel-consumption rate increases by many orders of magnitude as the temperature increases from T_s to T_∞.

For low ambient temperatures such that

$$B\exp\left(-\frac{E_a}{R_oT_\infty}\right) \ll \frac{D}{a^2} \tag{16}$$

the effect of pyrolysis is entirely negligible and the familiar results given in (4) and (5) are recovered. The following analysis considers instead the limiting case

$$B\exp\left(-\frac{E_a}{R_oT_s}\right) \ll \frac{D}{a^2} \ll B\exp\left(-\frac{E_a}{R_oT_\infty}\right), \tag{17}$$

when pyrolysis occurs in a thin layer centered at $r = r_f$ where the temperature is close to a value $T = T_f$, intermediate between T_s and T_∞. The thin reaction layer separates an inner region for $1 \le r < r_f$ where the flow is chemically frozen from an outer region for $r > r_f$ where the flow is in chemical equilibrium. The reciprocal of the dimensionless activation energy

$$\varepsilon = \left(\frac{E_a}{R_oT_f}\right)^{-1} \ll 1 \tag{18}$$

determines the characteristic thickness of the reaction layer $r - r_f \sim \varepsilon$ as well as the associated characteristic values of the fuel mass fraction $Y \sim \varepsilon$ and temperature variation $T - T_f \sim \varepsilon T_f$. Diffusion and chemical reaction are balanced in the reaction layer, a condition that leads to

$$\frac{B}{D/a^2}\left(\frac{E_a}{R_oT_f}\right)^{-2}\exp\left(-\frac{E_a}{R_oT_f}\right) \sim 1. \tag{19}$$

As revealed by the above order-of-magnitude estimate, in the limit of large activation energies the occurrence of the reaction at temperatures close to T_f implies that the frequency factor takes exponentially large values.

The solution in terms of matched-asymptotic expansions requires in principle introduction of the expansions

$$Y^- = Y_0^-(r) + \varepsilon Y_1^-(r) + \cdots \quad \text{and} \quad T^- = T_0^-(r) + \varepsilon T_1^-(r) + \cdots \tag{20}$$

in the frozen region $1 \le r \le r_f$ and

$$Y^+ = Y_0^+(r) + \varepsilon Y_1^+(r) + \cdots \quad \text{and} \quad T^+ = T_0^+(r) + \varepsilon T_1^+(r) + \cdots \tag{21}$$

in the equilibrium region $r_f \le r < \infty$, together with the reaction-layer expansions

$$Y = 0 + \varepsilon\varphi_1(\zeta) + \cdots \quad \text{and} \quad T = T_f + \varepsilon\theta_1(\zeta) + \cdots \tag{22}$$

involving the rescaled coordinate $\zeta = (r - r_f)/\varepsilon$. The analyses of the outer and inner regions are to be presented separately below.

5.2. The outer solution

For the specific case treated here the solution simplifies considerably. In particular, the existence of a positive temperature gradient $\mathrm{d}T^+/\mathrm{d}r|_{r=r_f} > 0$ on the equilibrium side of the reaction layer prevents fuel leakage at all orders, with the result that $Y_0^+ = Y_1^+ = \cdots = 0$. On the other hand, defining the pyrolysis-zone position r_f as the apparent fuel-depletion point as seen from the frozen region yields

$$\frac{\lambda}{r^2}\frac{\mathrm{d}Y^-}{\mathrm{d}r} - \frac{1}{L}\frac{1}{r^2}\frac{\mathrm{d}}{\mathrm{d}r}\left(r^2\frac{\mathrm{d}Y^-}{\mathrm{d}r}\right) = 0 \begin{cases} Y^-(1) = Y_s \\ Y^-(r_f) = 0 \end{cases} . \tag{23}$$

Substitution of the expansion for Y^- followed by integration of the problems found at increasing orders in powers of ε provides

$$\frac{Y^-}{Y_s} = \frac{Y_0^-}{Y_s} = \frac{e^{-L\lambda/r_f} - e^{-L\lambda/r}}{e^{-L\lambda/r_f} - e^{-L\lambda}}, \tag{24}$$

with all higher-order terms becoming identically zero (i.e. $Y_1^- = Y_2^- = \cdots = 0$). The result can be used in (12) to give

$$\lambda = \frac{\ln[1/(1-Y_s)]}{L(1-1/r_f)}, \tag{25}$$

relating the droplet vaporization rate $\lambda = \lambda Y_s - L^{-1}\mathrm{d}Y^-/\mathrm{d}r|_{r=1}$, equal to the fuel pyrolysis rate $-(r_f^2/L)\mathrm{d}Y/\mathrm{d}r|_{r=r_f}$, with the flame location r_f. Formally, the asymptotic problem in the limit $\varepsilon \ll 1$ is posed as that of finding the value of B that leads to a given value of r_f (or λ).

The outer temperature functions $T_n^\pm$ for $n = 0, 1, 2, \ldots$ satisfy the linear equations

$$\frac{\lambda}{r^2}\frac{\mathrm{d}T_n^\pm}{\mathrm{d}r} - \frac{1}{r^2}\frac{\mathrm{d}}{\mathrm{d}r}\left(r^2\frac{\mathrm{d}T_n^\pm}{\mathrm{d}r}\right) = 0, \tag{26}$$

obtained by neglecting the chemical term in (10). The boundary conditions on the frozen side are $T_0^- - T_s = T_1^- = T_2^- = \cdots = 0$ at $r = 1$ and $T_0^- - T_f = T_1^- - \theta_1^- = T_2^- - \theta_2^- = \cdots = 0$ at $r = r_f$, while the boundary conditions on the equilibrium side are $T_0^+ - T_\infty = T_1^+ = T_2^+ = \cdots = 0$ as $r \to \infty$ and $T_0^+ - T_f = T_1^+ - \theta_1^- = T_2^+ - \theta_2^- = \cdots = 0$ at $r = r_f$, where the constants θ_1^-, θ_1^+, etc are to be determined by matching the outer solution with the inner reactive layer. Straightforward integration of (26) provides

$$\frac{T_0^- - T_s}{T_f - T_s} = \frac{T_1^-}{\theta_1^-} = \frac{T_2^-}{\theta_2^-} = \cdots = \frac{e^{-\lambda/r} - e^{-\lambda}}{e^{-\lambda/r_f} - e^{-\lambda}} \tag{27}$$

and

$$\frac{T_\infty - T_0^+}{T_\infty - T_f} = \frac{T_1^+}{\theta_1^+} = \frac{T_2^+}{\theta_2^+} = \cdots = \frac{1 - e^{-\lambda/r}}{1 - e^{-\lambda/r_f}}. \tag{28}$$

The temperature description on the frozen side (27) can be used in (13) to evaluate the droplet heating rate, yielding at leading order

$$\frac{\dot{q}_d}{4\pi\kappa a L_v/c_p} = \lambda\left[\frac{c_p(T_f - T_s)/L_v}{e^{\lambda(1-1/r_f)} - 1} - 1\right]. \tag{29}$$

Additional useful equations, relating the different terms in (20) and (21), can be obtained by integrating once (14) and evaluating the result on both sides of the reaction layer, at intermediate distances $\varepsilon \ll |r - r_f| \ll 1$ where the outer expansions are valid. At leading order it is found that

$$\left.\frac{\mathrm{d}T_0^+}{\mathrm{d}r}\right|_{r=r_f} = \left.\frac{\mathrm{d}T_0^-}{\mathrm{d}r}\right|_{r=r_f} - \frac{q/c_p}{L}\left.\frac{\mathrm{d}Y_0^-}{\mathrm{d}r}\right|_{r=r_f}, \tag{30}$$

while at the following order

$$\lambda\, T_1^-\big|_{r=r_f} - r_f^2\left.\frac{\mathrm{d}T_1^-}{\mathrm{d}r}\right|_{r=r_f} = \lambda\, T_1^+\big|_{r=r_f} - r_f^2\left.\frac{\mathrm{d}T_1^+}{\mathrm{d}r}\right|_{r=r_f}. \tag{31}$$

Equation (30), stating that a fraction

$$\gamma = -\frac{q/c_p}{L}\left.\frac{\mathrm{d}Y_0^-}{\mathrm{d}r}\right|_{r=r_f} \Bigg/ \left.\frac{\mathrm{d}T_0^+}{\mathrm{d}r}\right|_{r=r_f} < 1 \tag{32}$$

of the heat reaching the reaction layer by conduction from the hot equilibrium region is employed to pyrolyze the fuel (the remaining heat being conducted towards the frozen region), can be evaluated with use made of (24), (27), and (28) to yield

$$\frac{T_f - T_s}{T_\infty - T_s} = \frac{e^{-\lambda/r_f} - e^{-\lambda}}{1 - e^{-\lambda}}\left[1 - \frac{q(e^{\lambda/r_f} - 1)}{c_p(T_\infty - T_s)}\right], \tag{33}$$

which can be used, together with (25), to determine T_f as a function of r_f. Similar evaluations of (31) and (32) provide

$$\frac{-\theta_1^-}{e^{\lambda} - e^{\lambda/r_f}} = \frac{\theta_1^+}{e^{\lambda/r_f} - 1}, \tag{34}$$

and

$$\gamma = \frac{q(e^{\lambda/r_f} - 1)}{c_p(T_\infty - T_f)}, \tag{35}$$

to be used in the following analysis.

5.3. The inner region

The problem in the inner region reduces to a reaction-diffusion balance, which can be described by rewriting (9) and (14) in terms of the rescaled variables, producing at leading order

$$\frac{\mathrm{d}^2 y_1}{\mathrm{d}\zeta^2} = \frac{BL}{\kappa/(\rho c_p a^2)}\left(\frac{E_a}{R_o T_f}\right)^{-2}\exp\left(-\frac{E_a}{R_o T_f}\right) y_1 e^{\theta_1/T_f}, \tag{36}$$

$$\frac{\mathrm{d}^2}{\mathrm{d}\zeta^2}\left(\theta_1 - \frac{q/c_p}{L}y_1\right) = 0. \tag{37}$$

Note that the factor affecting the reaction term reflects the anticipated scaling (19). Matching with the outer solutions provides the boundary conditions

$$y_1 = \left(\left. \frac{\mathrm{d}Y_0^-}{\mathrm{d}r} \right|_{r=r_f} \right) \zeta; \quad \theta_1 - \left(\left. \frac{\mathrm{d}T_0^-}{\mathrm{d}r} \right|_{r=r_f} \right) \zeta = \theta_1^- \qquad \text{as} \quad \zeta \to -\infty, \tag{38}$$

$$y_1 = 0; \quad \theta_1 - \left(\left. \frac{\mathrm{d}T_0^+}{\mathrm{d}r} \right|_{r=r_f} \right) \zeta = \theta_1^+ \qquad \text{as} \quad \zeta \to +\infty. \tag{39}$$

Integrating (37) readily yields

$$\theta_1 - \frac{q/c_p}{L} y_1 = \left(\left. \frac{\mathrm{d}T_0^+}{\mathrm{d}r} \right|_{r=r_f} \right) \zeta + \theta_1^+ = \left(\left. \frac{\mathrm{d}T_0^-}{\mathrm{d}r} \right|_{r=r_f} - \frac{q/c_p}{L} \left. \frac{\mathrm{d}Y_0^-}{\mathrm{d}r} \right|_{r=r_f} \right) \zeta + \theta_1^-, \tag{40}$$

relating the temperature and fuel mass fraction in the reaction layer. The condition $\theta_1^+ = \theta_1^-$, stemming from the above expression and (30), and that stated in (34) can be simultaneously satisfied only if $\theta_1^+ = \theta_1^- = 0$, revealing that, just like the fuel mass fraction, the temperature has zero first-order corrections in the frozen and equilibrium regions.

Using (40) with $\theta_1^+ = \theta_1^- = 0$ and introducing for convenience the rescaled variables

$$\varphi = \frac{q}{c_p T_f} \frac{y_1}{L} \quad \text{and} \quad \eta = \frac{\lambda}{r_f^2} \frac{q}{c_p T_f} \zeta \tag{41}$$

along with the rescaled Damköhler number

$$\Delta = \frac{B}{D/a^2} \left(\frac{E_a}{R_o T_f} \right)^{-2} \left(\frac{\lambda}{r_f^2} \right)^{-2} \left(\frac{q}{c_p T_f} \right)^{-2} \exp\left(-\frac{E_a}{R_o T_f} \right) \tag{42}$$

results in the boundary-value problem

$$\frac{\mathrm{d}^2 \varphi}{\mathrm{d}\eta^2} = \Delta \varphi e^{\varphi + \eta/\gamma}; \quad \begin{cases} \varphi + \eta = 0 \text{ as } \eta \to -\infty \\ \varphi = 0 \text{ as } \eta \to +\infty \end{cases} . \tag{43}$$

Note that the condition $\varphi + \eta = 0$ as $\eta \to -\infty$ effectively implies that $\mathrm{d}\varphi/\mathrm{d}\eta - 1$ must approach zero, so that for a given γ the above second-order equation must satisfy three boundary conditions, which is possible only for a single value of $\Delta(\gamma)$, the eigenvalue of the problem. The mathematical problem defined in (43) is similar to that encountered in Liñán's classical premixed-flame regime of nonpremixed combustion [16]. Despite the similarity, however, reduction to the same canonical form in general is not feasible, the only exception being the limit $\gamma \ll 1$, in which the solution to (43) can be related at leading order to one of the limiting cases considered by Liñán, as shown below.

5.4. Solution to the canonical problem

For a given positive value of $\gamma < 1$, defined in (32), the profiles of $\varphi(\eta)$ and corresponding values of Δ were obtained by a shooting integration scheme initiated at $-\eta \gg 1$. The resulting variation of Δ with γ is shown in Fig. 3 along with selected profiles of $\varphi(\eta)$ for $\gamma = 0.2$ and $\gamma = 0.99$. The numerical integration is more difficult for $\gamma \ll 1$, when the reaction layer becomes very thin, and also for $1 - \gamma = (\mathrm{d}T_0^-/\mathrm{d}r|_{r=r_f})/(\mathrm{d}T_0^+/\mathrm{d}r|_{r=r_f}) \ll 1$, when the temperature gradient on the frozen side is very small, with the consequence that the reaction extends far into the frozen region. Useful analytic predictions for $\Delta(\gamma)$ in these two limiting cases are presented below.

For $\gamma \ll 1$, introducing the rescaled variables $\bar{\varphi} = \varphi/\gamma$, $\bar{\eta} = \eta/\gamma$, and $\bar{\Delta} = \gamma^2\Delta$ and neglecting small terms of order γ reduces (43) to the linear problem

$$\frac{\mathrm{d}^2\bar{\varphi}}{\mathrm{d}\bar{\eta}^2} = \bar{\Delta}\bar{\varphi}e^{\bar{\eta}}; \quad \begin{cases} \bar{\varphi} + \bar{\eta} = 0 & \text{as } \bar{\eta} \to -\infty \\ \bar{\varphi} = 0 & \text{as } \bar{\eta} \to +\infty \end{cases}, \tag{44}$$

which can be written in the standard form

$$\frac{\mathrm{d}^2\bar{\varphi}}{\mathrm{d}z^2} + \frac{1}{z}\frac{\mathrm{d}\bar{\varphi}}{\mathrm{d}z} - \bar{\varphi} = 0; \quad \begin{cases} \bar{\varphi} = -2\left[\ln(z/2) - \ln(\bar{\Delta})/2\right] & \text{as } z \to 0 \\ \bar{\varphi} = 0 & \text{as } z \to \infty \end{cases}, \tag{45}$$

involving $z = 2\sqrt{\bar{\Delta}e^{\bar{\eta}}}$ as independent variable. The general solution to the above equation can be expressed as a linear combination of the modified Bessel functions of zeroth order, $\bar{\varphi} = C_K\mathrm{K}_0(z) + C_I\mathrm{I}_0(z)$, involving the constants of integration C_K and C_I. The boundary condition as $z \to \infty$ requires that $C_I = 0$, while the boundary condition as $z \to 0$ provides $C_K = 2$ and

$$\bar{\Delta} = e^{-2\gamma_E} \simeq 0.315236, \tag{46}$$

where $\gamma_E \simeq 0.577215$ represents Euler's constant. It is worth noting that the same mathematical problem was encountered by Liñán in one of the limiting solutions to the premixed-flame regime, namely, the limit $-m \to \infty$ discussed in Appendix C of [16]. As seen in the comparison of Fig. 3, the leading-order result $\Delta = 0.315236\gamma^{-2}$ predicts the Damköhler number for $\gamma \ll 1$ with small relative errors of order γ.

As illustrated in the upper inset of Fig. 3, for $1 - \gamma \ll 1$ the solution exhibits a fuel-depletion layer with order-unity thickness centered about $\eta = \eta_o \gg 1$. As is apparent from (43), this displacement is consistent with a small value of $\Delta \ll 1$, such that $\eta_o \sim \ln(1/\Delta)$, as needed to enable a diffusion-reaction balance to be preserved. The rescaled fuel mass fraction, of order $\varphi \sim 1$ for $\eta - \eta_o \sim 1$, increases towards the frozen side, giving characteristic values of $\varphi + \eta \sim \ln(1/\Delta)$ at distances $-\eta \sim 1$. The chemical reaction continues in a region that extends for $-\eta \sim (1-\gamma)^{-1} \gg 1$ with $\varphi + \eta \sim 1$. In this weakly reactive region, which ultimately determines the value of Δ, the diffusion-reaction equation takes the form

$$\frac{\mathrm{d}^2\hat{\varphi}}{\mathrm{d}\hat{\eta}^2} = -\hat{\Delta}\hat{\eta}e^{\hat{\varphi}+\hat{\eta}} \tag{47}$$

when written in terms of the rescaled variables $\hat{\varphi} = \varphi + \eta$, $\hat{\eta} = (1-\gamma)\eta$, and $\hat{\Delta} = \Delta/(1-\gamma)^3$. The solution must satisfy $\hat{\varphi} = 0$ and $\mathrm{d}\hat{\varphi}/\mathrm{d}\hat{\eta} = 0$ as $\hat{\eta} \to -\infty$ and must match as $\hat{\eta} \to 0$ with the solution encountered for $-\eta \sim 1$.

Integration of (47) from $-\hat{\eta} \gg 1$ reveals that for $\hat{\Delta}$ larger than a critical value $\hat{\Delta}_c \simeq 1.1517$ the solution develops a singularity before reaching $\hat{\eta} = 0$, i.e. $\hat{\varphi} \to +\infty$ at a negative value of $\hat{\eta}$, while for $\hat{\Delta} < \hat{\Delta}_c$ the integration reaches $\eta = 0$ with $\hat{\varphi} \sim 1$. It is clear that a consistent asymptotic description, including matching with the solution in the intermediate region $-\eta \sim 1$ where $\hat{\varphi} \sim \ln(1/\Delta) \gg 1$, is only possible for $\hat{\Delta} = \hat{\Delta}_c \simeq 1.1517$, for which the singularity of the outer solution develops exactly at $\hat{\eta} = 0$. The analysis of the weakly reactive region therefore provides the asymptotic prediction $\Delta = \hat{\Delta}_c(1-\gamma)^3$ for $1 - \gamma \ll 1$. It is remarkable how this leading-order result can be derived without analyzing in detail the multi-layer structure of the solution near $\eta = 0$. Such an analysis would be necessary, however, in deriving higher-order corrections, but these do not appear to be needed, in view of the excellent accuracy of the leading-order prediction $\Delta = 1.1517(1-\gamma)^3$, demonstrated by the comparison seen in Fig. 3.

6. The pyrolysis temperature

For known values of the pyrolysis-rate parameters B and E_a, the preceding description of the quasi-steady gas flow surrounding the droplet can be coupled with (1) and (2), describing the temperature variation inside the droplet $T_d(\tilde{r}, t)$ and the droplet radius $a(t)$, to enable predictions of droplet-vaporization histories to be made. In the calculation, the Clasius-Clapeyron equation (3) is used to determine Y_s as a function of the instantaneous droplet-surface temperature T_s. The result can be used in solving (25), (29), (33), (35), and (42), supplemented by the function $\Delta(\gamma)$ shown in Fig. 3, to determine λ, $\dot{q}_d$, r_f, T_f, γ, and Δ. The analysis simplifies at the end of the droplet-heating period, when the droplet temperature reaches a uniform constant value $T_d = T_s$, close to T_B when $L_v/(R_F T_B) \gg 1$. During this stage the droplet heating rate $\dot{q}_d$ is identically zero, while λ, Y_s, T_s, r_f, T_f, γ, and Δ reach values that remain almost constant, with the square of the droplet radius changing linearly with time according to (7). This constant slope is clearly visible in the plots of Fig. 2.

The calculation procedure outlined above can be simplified by exploiting further the strong temperature sensitivity of the chemical reaction, entering in the theoretical description through the exponential present in (42). It can be reasoned that for large values of the dimensionless activation energy $E_a/(R_o T_f) \gg 1$ the relative changes in T_f are limited to small values of order $[E_a/(R_o T_f)]^{-1} \ll 1$. Therefore, at leading order in the limit $E_a/(R_o T_f) \gg 1$ the pyrolysis temperature T_f of a given fuel becomes a constant kinetic parameter, which takes the same value regardless of the droplet radius a or ambient temperature T_∞, with pyrolysis becoming negligible when $T_\infty < T_f$.

The value of T_f can be obtained from measurements of the constant slope of the curve $\mathrm{d}a^2/\mathrm{d}t$ reached at the end of the droplet-heating period. The computation begins by writing (7) in the form

$$\lambda = -\frac{\rho_l c_p}{2\kappa}\frac{\mathrm{d}a^2}{\mathrm{d}t}, \tag{48}$$

while setting $\dot{q}_d = 0$ in (29), and combining the result with (33) provides

$$\frac{T_f - T_s}{L_v/c_p} = \frac{(q + L_v)(e^\lambda - 1) - c_p(T_\infty - T_s)}{q + c_p(T_\infty - T_s) - L_v(e^\lambda - 1)} \tag{49}$$

and

$$r_f = \lambda \ln^{-1}\left[1 + \frac{c_p(T_\infty - T_s) - L_v(e^\lambda - 1)}{q}\right]. \tag{50}$$

The above three equations, together with (3) and (25), constitute a coupled system of equations that determine T_f along with the associated values of λ, Y_s, T_s, and r_f. The solution can be obtained by a simple iterative scheme. Since κ has a very weak dependence on Y_s, while $T_B - T_s \ll T_B$, as follows from (3) when $L_v/(R_F T_B) \gg 1$, one may use (48) with ρ_l, c_p, κ evaluated with use made of $T_s = T_B$ and an estimated value of Y_s to compute λ, which can be substituted into (49) to determine T_f in the first approximation. A correction can be obtained by using the value of r_f given by (50) to evaluate Y_s from (25) and substituting the result into (3) to obtain T_s. These new values of Y_s and T_s can then be used in (48) to recompute λ, leading to a more accurate evaluation of T_f from (49).

This simple iterative procedure was used to determine the values of T_f corresponding to the three alkanes of Fig. 2 from the slope of the curve $\mathrm{d}a^2/\mathrm{d}t$ corresponding to $T_\infty = 1730$ K, yielding the values $T_f =$(1080 K, 912 K, 841 K) for heptane, dodecane and hexadecane, respectively, with associated reaction-zone standoff ratios given by $r_f = (7.34, 4.95, 4.14)$. Because of the strong temperature sensitivity of the pyrolysis reaction, it is expected that the values of T_f evaluated from the experiments at a different value of T_∞ should differ by a small relative amount of order $[E_a/(R_o T_f)]^{-1}$ from the values given above, whereas the corresponding value of r_f could in principle differ by an amount of order unity. To check for consistency, the values of T_f and r_f corresponding to hexadecane were recomputed using the slope $-\mathrm{d}a^2/\mathrm{d}t$ corresponding to $T_\infty = 1311$ K, yielding $T_f = 969$ K and $r_f = 9.86$, to be compared with the values $T_f = 841$ K and $r_f = 4.14$ obtained at high temperature. The differences in T_f, 128 K, appear to be consistent with the effective dimensionless activation energy being on the order of $E_a/(R_o T_f) \sim 10$ for hexadecane.

The fraction γ of the heat conducted from the ambient atmosphere that is employed in fuel pyrolysis, as defined in (32) and calculated from (35), is appreciable, being (0.486, 0.591, 0.670) for heptane, dodecane and hexadecane, respectively at $T_\infty = 1730$ K. This is consistent with the pyrolysis energy q being large compared with the heat of vaporization L_v and with T_f not being very much less than T_∞, so that the discontinuity in the temperature gradient at the pyrolysis zone is mild, that zone being situated far enough from the surface of the droplet that its standoff ratio r_f, which depends strongly on T_f, is not small in these experiments. The corresponding "pyrolysis dip" observed in liquid-fuel combustion is much closer to the liquid surface, remaining, however, similarly small, the pyrolysis energy being typically much less than heats of combustion. The concept of a pyrolysis temperature in fact may also find application on the fuel side of diffusion flames in combustion experiments, although this application has not been explored yet. The interest in the present work, however, is restricted to vaporization.

7. The modified Spalding law

With errors of order $[E_a/(R_oT_f)]^{-1}$, predictions of droplet vaporization histories based on treating T_f as a fixed kinetic property of the fuel can make use of (25) and (33) to obtain λ and r_f for given values of T_s, Y_s, and T_∞, with $\dot{q}_d$ following from (29). In particular, the constant value of λ reached when $\dot{q}_d = 0$ at the end of the droplet-heating period is given by

$$\lambda = \ln\left[1 + \frac{c_p(T_\infty - T_s)}{L_v} - \left(\frac{q}{L_v}\right)\left(\frac{c_p(T_\infty - T_f)}{q + L_v + c_p(T_f - T_s)}\right)\right], \tag{51}$$

as can be seen by solving (49) for λ. If the approximation $T_s = T_B$ is used, then the above expression allows us to quantify directly the reduced vaporization rate associated with fuel pyrolysis, which enters as a correction proportional to q/L_v that vanishes at $T_\infty = T_f$.

In interpreting the result, it is convenient to rewrite (51) in the alternative form

$$\lambda = \ln\left[1 + \frac{c_p(T_a - T_s)}{L_v}\right], \tag{52}$$

where the apparent temperature of the atmosphere is

$$T_a = \alpha T_f + (1 - \alpha)T_\infty \tag{53}$$

with

$$\alpha = \frac{q}{L_v + c_p(T_f - T_s) + q}. \tag{54}$$

As can be seen by comparing the above expression with the classical Spalding solution (6), the presence of pyrolysis results in the modified effective ambient temperature T_a, intermediate between T_f and T_∞. As seen in (54), the weighting factor α is the ratio of the amount of heat involved in the fuel pyrolysis to the total amount needed to vaporize the liquid fuel, heat up the resulting vapor to the pyrolysis temperature T_f, and pyrolyze it. The values of α corresponding to T_f =(1080 K, 912 K, 841 K) can be evaluated using an approximate specific heat $c_p = 3.7 \times 10^3$ J/(kg K) along with $T_s = T_B$ =(371 K, 489 K, 560 K) to give $\alpha = (0.48, 0.60, 0.70)$ for heptane, dodecane, and hexadecane, respectively (evaluations of α accounting for departures of T_s from T_B and using the "1/3 rule" [13] for computing c_p yield values that differ by about 1 % from those given above). As can be seen, the effect of pyrolysis is more important for heavier alkanes, for which the apparent temperature is closer to the pyrolysis temperature, thereby having a larger impact on the vaporization rate (52).

As a further check on the accuracy of the T_f =constant approximation, the value of $\alpha = 0.70$ evaluated for hexadecane with $T_f = 841$ K (the value obtained from the experiments at $T_\infty = 1730$ K) was used in (52) to provide a prediction for the vaporization rate at $T_\infty = 1311$ K. The associated slope $-\mathrm{d}a^2/\mathrm{d}t$, evaluated from (7), was found to be $-\mathrm{d}a^2/\mathrm{d}t = 0.1049$ mm^2/s, which differs by 9.2 % from the value $-\mathrm{d}a^2/\mathrm{d}t = 0.1156$ mm^2/s determined experimentally. This small departure is again consistent with the errors, of order $[E_a/(R_oT_f)]^{-1}$, present in the leading-order description considered here.

8. Concluding remarks

The experimental results reported here have shown how fuel-pyrolysis effects reduce vaporization rates of normal alkanes, to an increasing extent with increasing chain length of the fuel molecule. A new theory of droplet vaporization has been developed to quantify the resulting vaporization-rate decrease. The needed one-step endothermic activation-energy analysis differs markedly from previous activation-energy analysis, which considered only exothermic reactions. It involves complexities that may not initially be anticipated, such as an extended weakly reactive layer in the inner zone when a large fraction of the heat conducted from the ambient atmosphere is required for pyrolysis. The kinetically controlled pyrolysis temperature T_f is seen to emerge as a useful kinetic approximation that replaces at leading order the Arrhenius parameters B and E_a. Determination of E_a and subsequently B from measurements of vaporization rates at different T_∞ would require accuracies of 1% or better because of their strong sensitivity to vaporization-rate changes. This underscores the importance of the kinetically controlled pyrolysis temperature in interpreting experimental droplet-vaporization results.

The analysis reveals that pyrolysis effects are absent for droplets vaporizing in low-temperature atmospheres with temperatures T_∞ below T_f. Formulas are developed for the vaporization and heating rates of droplets vaporizing in high-temperature atmospheres with $T_\infty > T_f$. At the end of the heat-up period, when the droplet temperature reaches a constant value, the equation for the vaporization rate accounting for the presence of pyrolysis can be cast in the classical form (52) originally derived by Godsave and Spalding [5, 6], with the ambient temperature T_∞ replaced by the apparent ambient temperature $T_a = \alpha T_f + (1 - \alpha)T_\infty$, involving the fuel-specific energetic weighting factor α defined in (54). Clearly, additional experiments involving different levels of ambient temperature and different alkanes should be considered in future work to test the accuracy of the predictive formulae derived here and improve the evaluation of the pyrolysis temperature T_f. Besides droplet experiments, counterflow systems involving liquid fuel pools or prevaporized alkane jets and preheated inert gases can be useful in that respect, providing insightful information free from transient effects.

9. Acknowledgments

The work of AM and JB was supported by the Spanish Ministry of Education through the pre-doctoral grant FPU15/01866 and the Spanish Ministry of Economy and Competitiveness and European Union FEDER funds through research project ENE2016-76436-R. The work of JC was supported through the Ministerio de Ciencia, Innovación y Universidades through project # PGC2018-097565-B-I00 and through travel grant # CAS18/00426. The help of Luis Ojeda and Diego Aranda with the droplet evaporation tests and of Dr. Antonio Lozano with the PIV measurements is also gratefully acknowledged.

References

[1] W. A. Sirignano, Fuel droplet vaporization and spray combustion theory, Prog. Energ. Combust. Sci. 9 (4) (1983) 291–322.

[2] C. K. Law, Recent advances in droplet vaporization and combustion, Prog. Energ. Combust. Sci. 8 (3) (1982) 171–201.
[3] G. Godsave, Combustion of droplets in a fuel spray, Nature 164 (4173) (1949) 708.
[4] D. B. Spalding, Combustion of liquid fuels, Nature 165 (4187) (1950) 160–160.
[5] G. Godsave, Studies of the combustion of drops in a fuel spray—the burning of single drops of fuel, in: Proc. Combust. Inst., Vol. 4, Elsevier, 1953, pp. 818–830.
[6] D. Spalding, The combustion of liquid fuels, in: Proc. Combust. Inst., Vol. 4, Elsevier, 1953, pp. 847–864.
[7] W. A. Sirignano, Fluid dynamics and transport of droplets and sprays, 2nd Edition, Cambridge University Press, 2010.
[8] A. L. Sánchez, J. Urzay, A. Liñán, The role of separation of scales in the description of spray combustion, Proc. Combust. Inst. 35 (2) (2015) 1549–1577.
[9] B. Abramzon, W. Sirignano, Droplet vaporization model for spray combustion calculations, Int. J. Heat Mass Transf. 32 (9) (1989) 1605–1618.
[10] A. Crespo, A. Liñán, Unsteady effects in droplet evaporation and combustion, Combust. Sci. Technol. 11 (1-2) (1975) 9–18.
[11] Á. Muelas, P. Remacha, J. Ballester, Droplet combustion and sooting characteristics of uco biodiesel, heating oil and their mixtures under realistic conditions, Combust. Flame 203 (2019) 190–203.
[12] T. Li, D. Zhu, N. Akafuah, K. Saito, C. K. Law, Synthesis, droplet combustion, and sooting characteristics of biodiesel produced from waste vegetable oils, Proc. Combust. Inst. 33 (2) (2011) 2039–2046.
[13] G. Hubbard, V. Denny, A. Mills, Droplet evaporation: effects of transients and variable properties, Int. J. Heat Mass Transf. 18 (9) (1975) 1003–1008.
[14] R. J. Kee, G. Dixon-Lewis, J. Warnatz, M. E. Coltrin, J. A. Miller, A fortran computer code package for the evaluation of gas-phase multicomponent transport properties, Sandia National Laboratories Report SAND86-8246 13 (1986) 80401–1887.
[15] P. E. Savage, Mechanisms and kinetics models for hydrocarbon pyrolysis, J. Anal. Appl. Pyrol. 54 (1-2) (2000) 109–126.
[16] A. Liñán, The asymptotic structure of counterflow diffusion flames for large activation energies, Acta Astronautica 1 (7-8) (1974) 1007–1039.

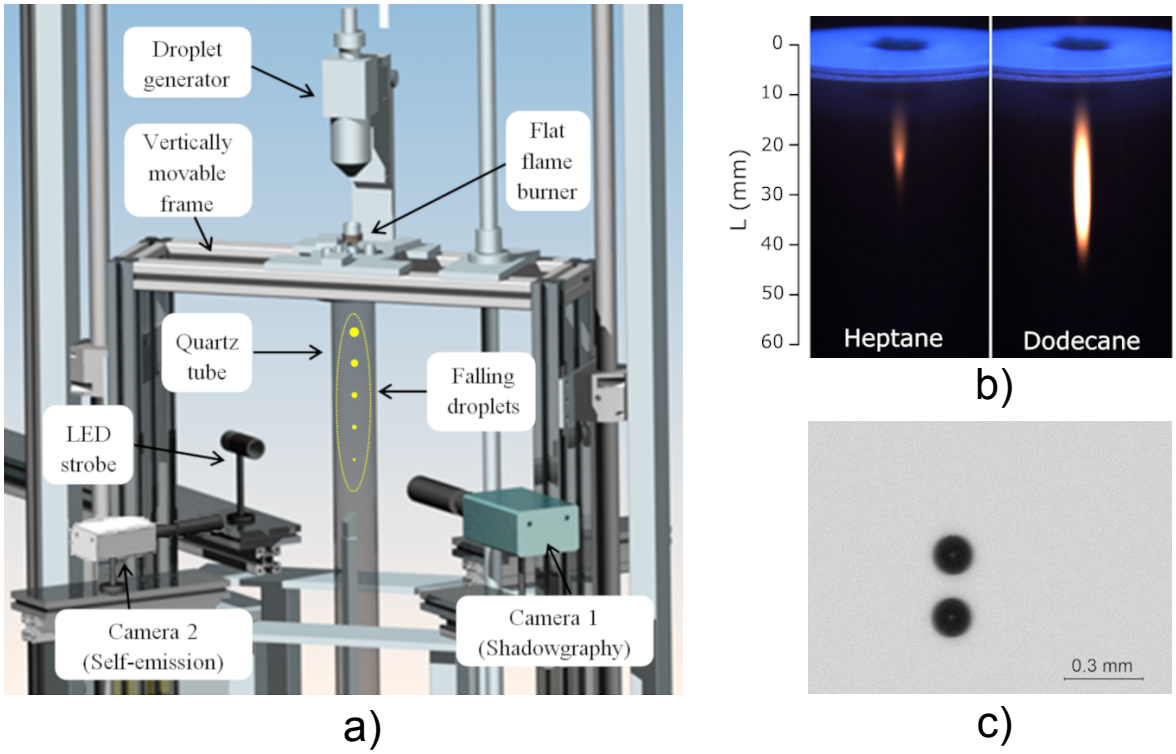

Figure 1: A schematic view of the experimental facility employed in this paper (a). The pictures on the right-hand side corresponds to macroscopically visible traces created by soot thermal emission for the heptane and dodecane tests (b) and to double-exposure photography of a free-falling hexadecane droplet (c).

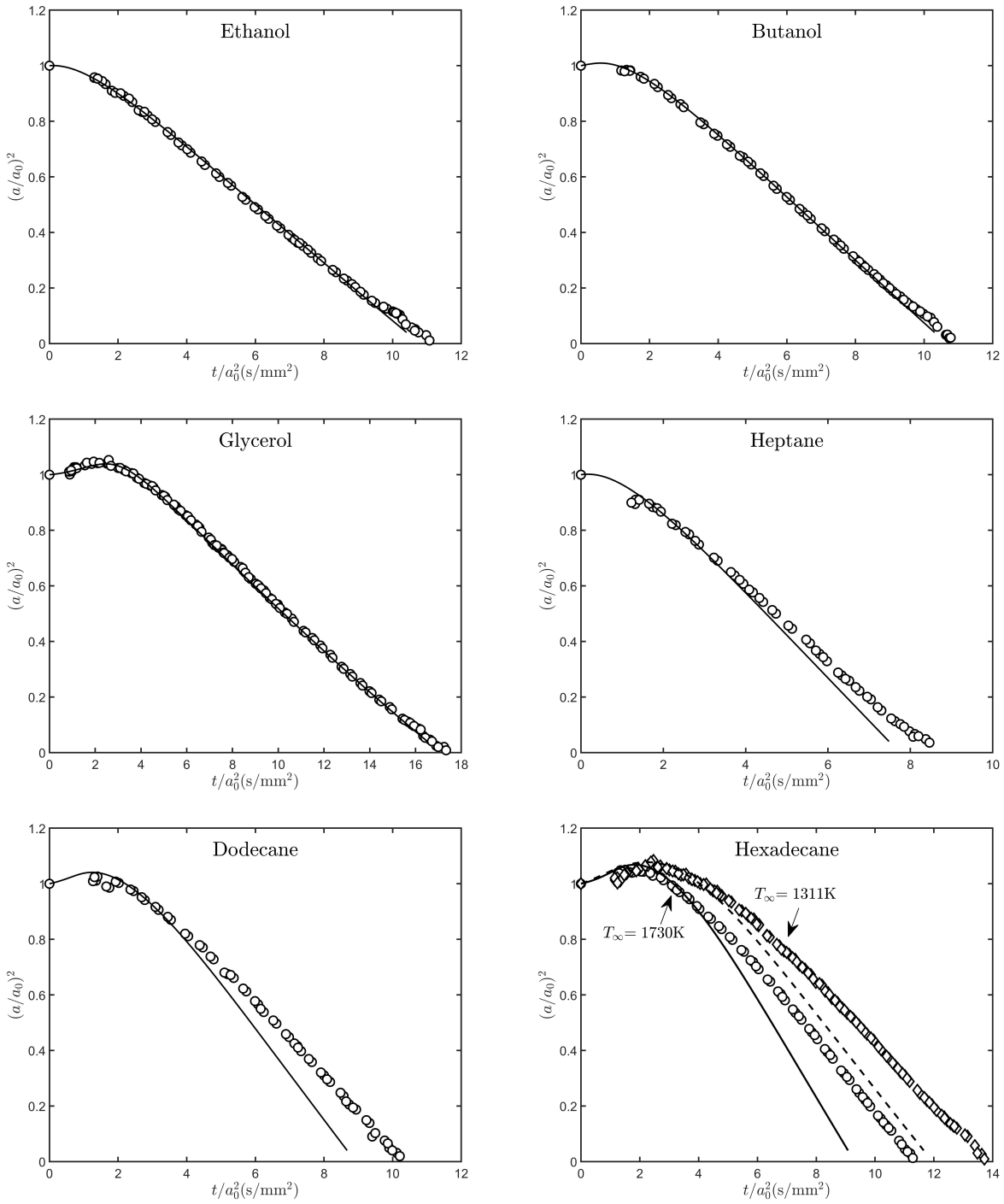

Figure 2: The variation with time of the droplet radius as obtained from post-processing the images taken at different distances from the injection point (symbols) and as obtained with the theoretical predictions corresponding to vaporization of a spherical droplet in a quasi-steady chemically frozen gaseous atmosphere. In all cases, the target temperature of the gaseous coflow was $T_\infty = 1730$ K, with additional results given for hexadecane at $T_\infty = 1311$ K.

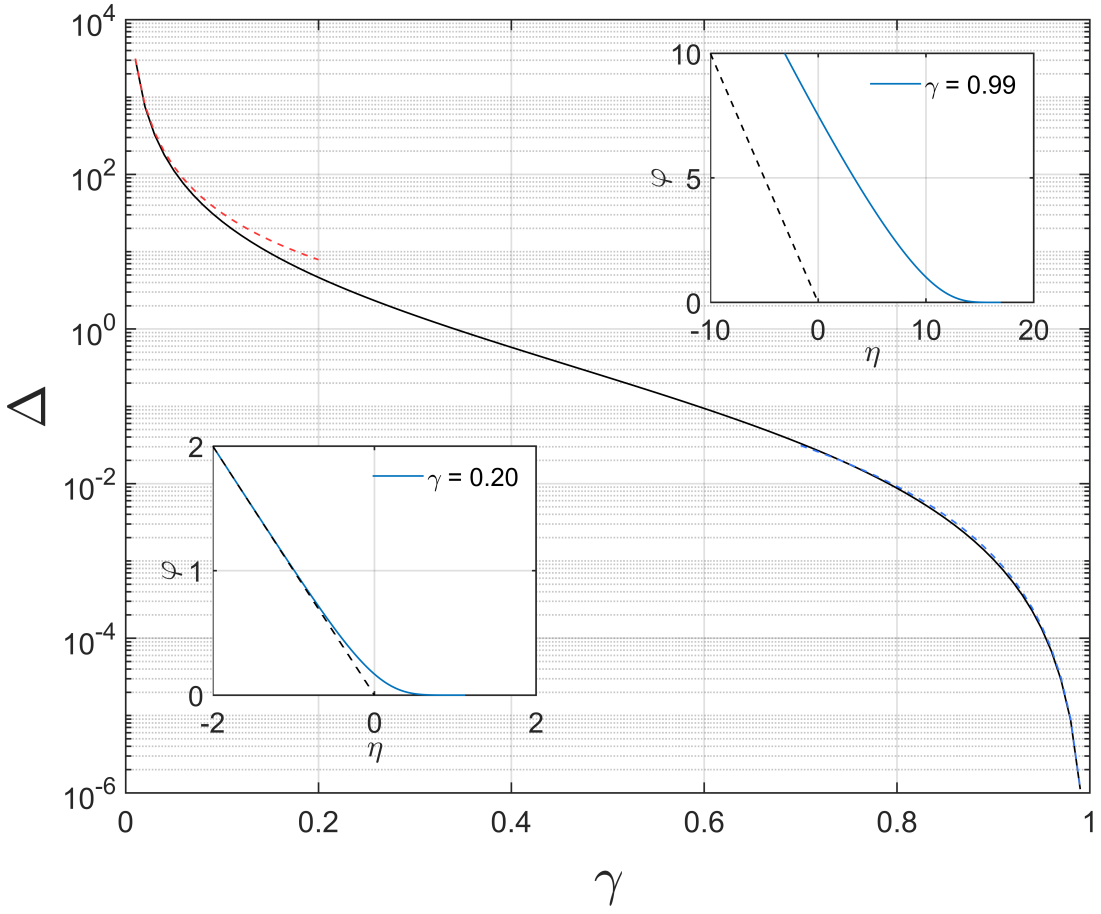

Figure 3: The variation of Δ with γ as obtained from numerical integration of the eigenvalue problem (43) (solid curve) and the asymptotic predictions $\Delta = 0.315236\gamma^{-2}$ for $\gamma \ll 1$ and $\Delta = 1.1517(1-\gamma)^3$ for $1-\gamma \ll 1$ (dashed curves). The insets show the profiles of reduced fuel mass fraction $\varphi(\eta)$ for $\gamma = 0.2$ and $\gamma = 0.99$, with the dashed lines representing the asymptotes $\varphi = -\eta$.

Figure 1

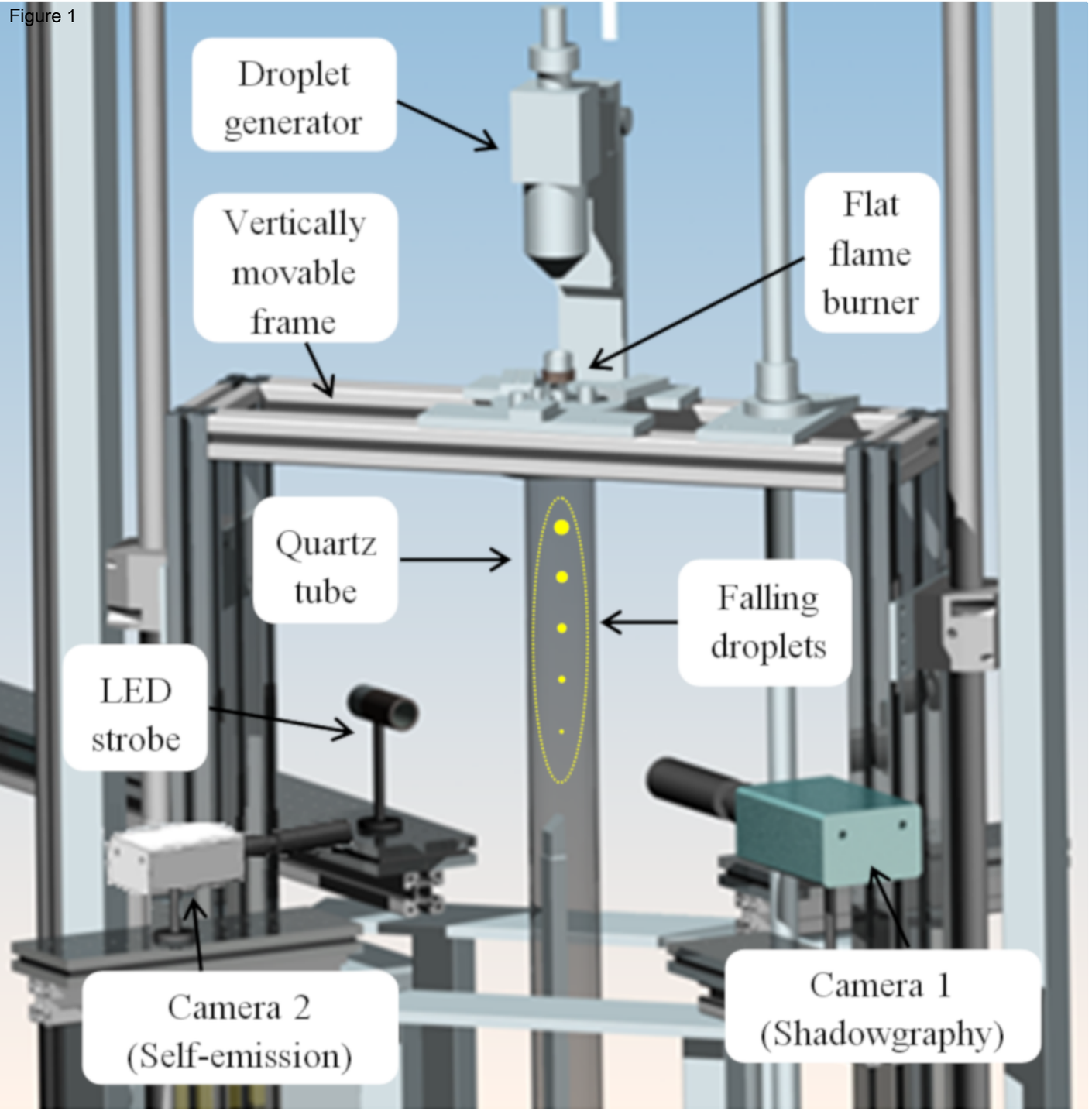

a)

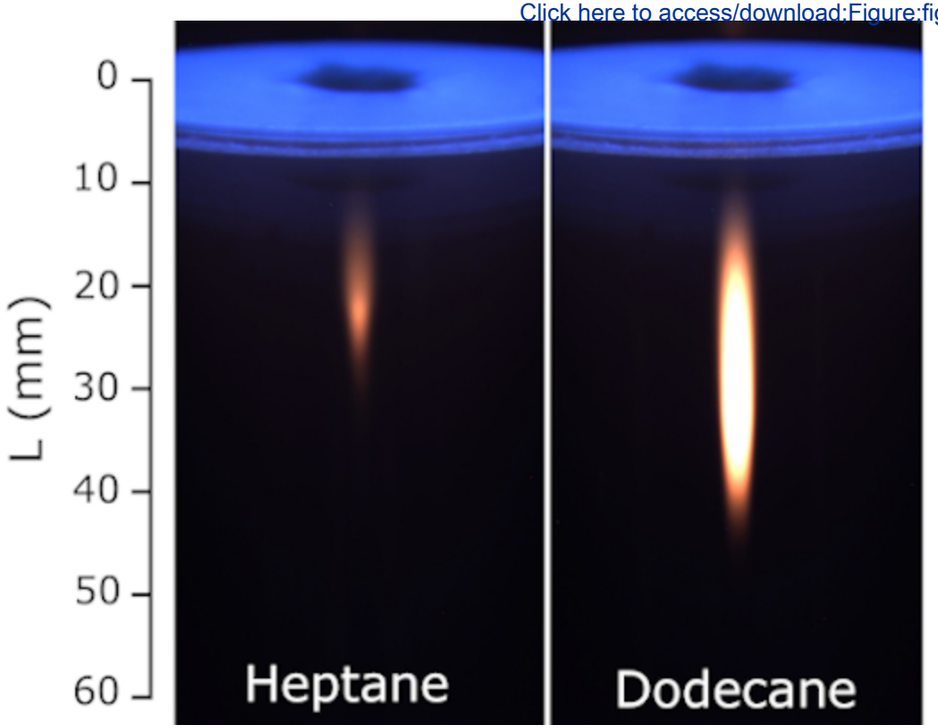

b)

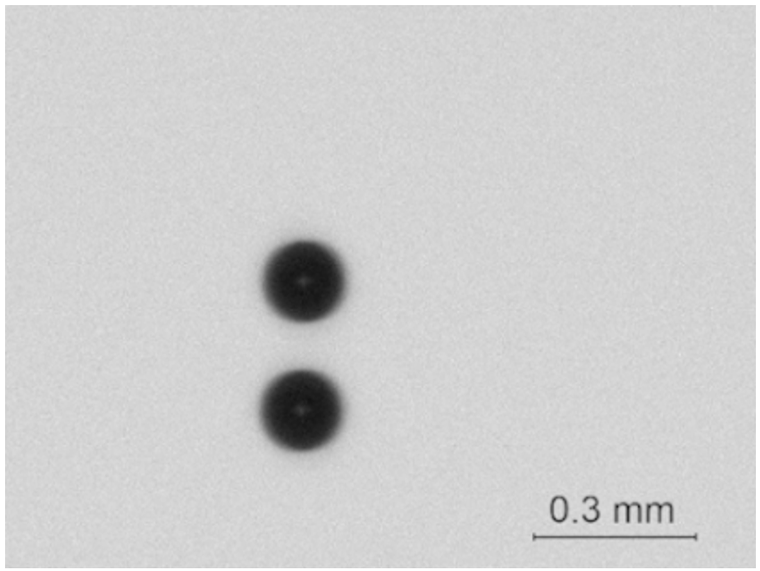

c)

Figure 2

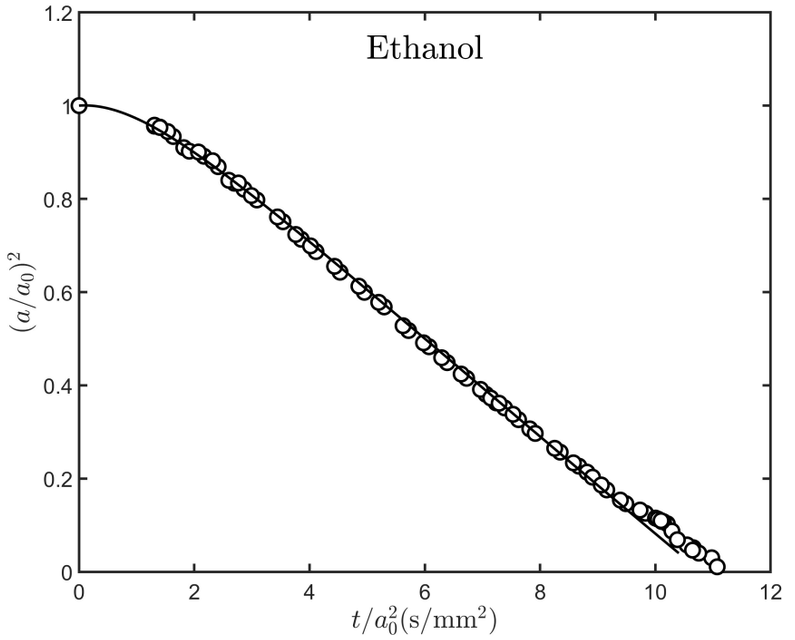

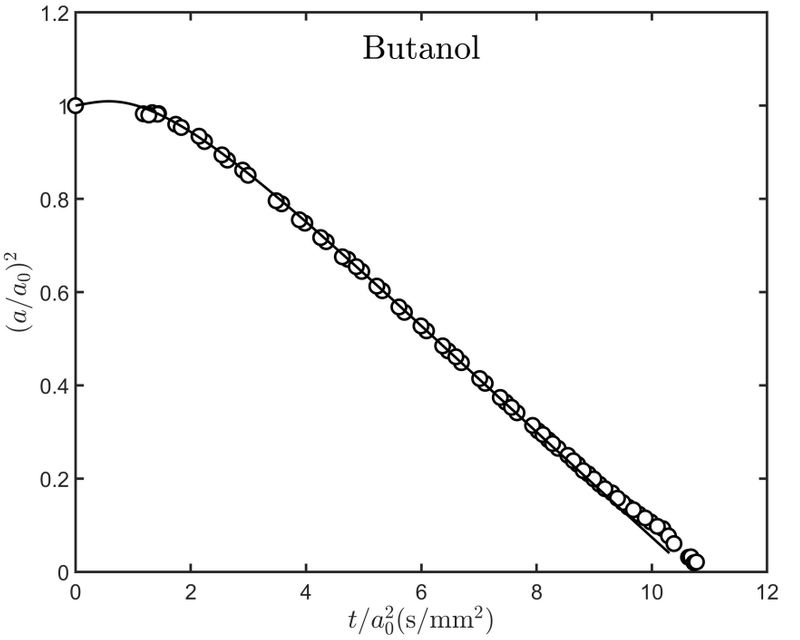

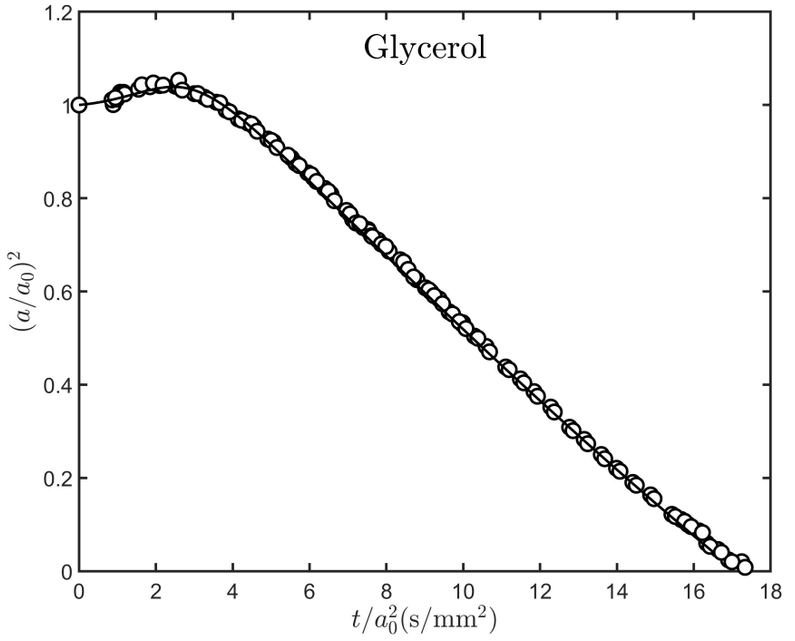

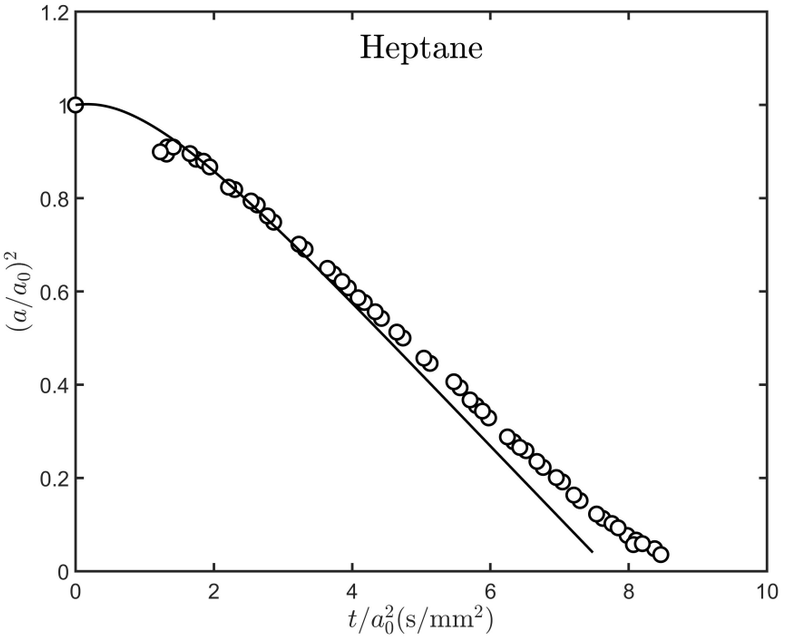

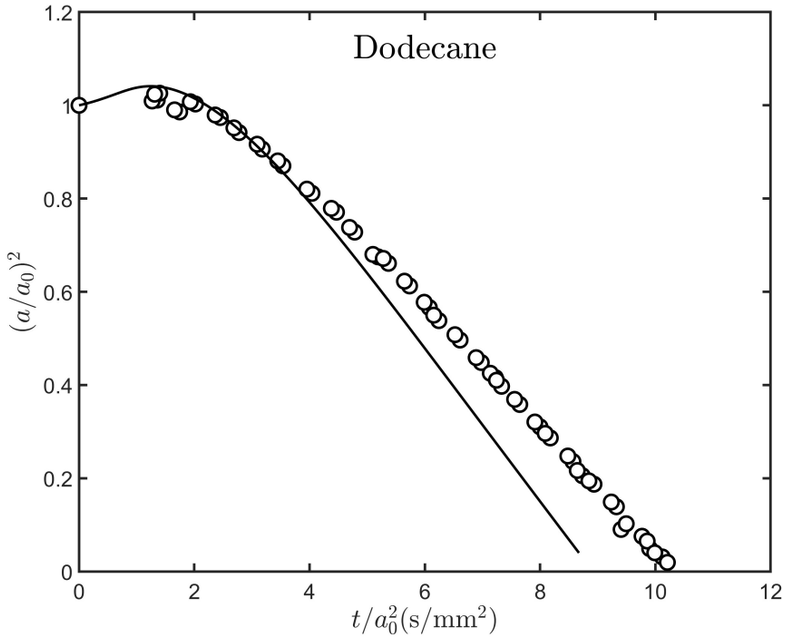

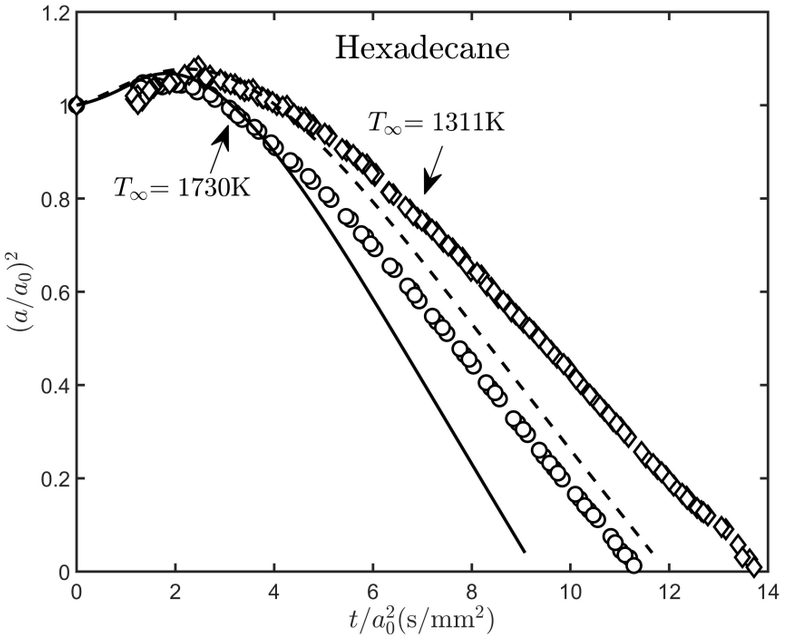

Figure 3

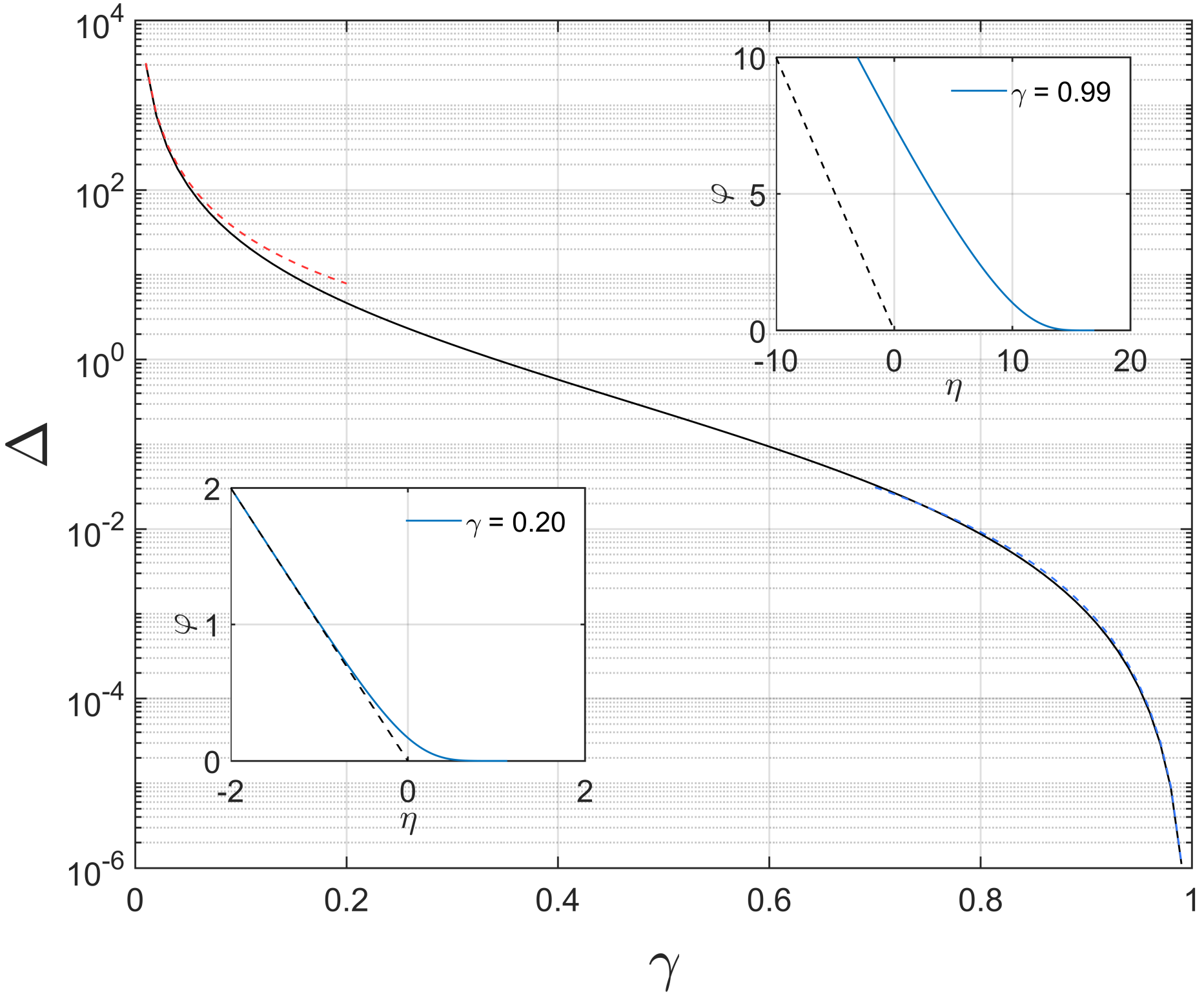

Declaration of interests

☒ The authors declare that they have no known competing financial interests or personal relationships that could have appeared to influence the work reported in this paper.

☐ The authors declare the following financial interests/personal relationships which may be considered as potential competing interests: